IET Electrical Systems in Transportation

Special Issue: Design, Modeling and Control of Electric Vehicles: Selected Papers from IEEE Vehicle Power and Propulsion Conference (VPPC 2015)

IET Journals
The Institution of Engineering and Technology

Electric vehicle drivetrain optimisation

ISSN 2042-9738
Received on 6th March 2016
Revised 11th May 2016
Accepted on 1st June 2016
E-First on 8th July 2016
doi: 10.1049/iet-est.2016.0022
www.ietdl.org

Jony J. Eckert[1] ✉, Ludmila C.A. Silva[1], Eduardo S. Costa[1], Fabio M. Santiciolli[1], Franco G. Dedini[1], Fernanda C. Corrêa[2]

[1]Integrated Systems Department, State University of Campinas – UNICAMP, 200 Mendeleyev Street, Campinas, Brazil
[2]Electrical Engineering Department, Federal Technological University of Paraná – UTFPR, Monteiro Lobato Avenue – Jardim Carvalho Ponta Grossa, Ponta Grossa, Brazil
✉ *E-mail: javorski@fem.unicamp.br*

Abstract: This study provides a detailed analysis of an optimal drivetrain configuration, based on multi-cycles, for a plug-in electric vehicle (EV). The investigation aims to identify the best EV configuration according to the required power and the transmissible traction torque. The study focuses on an EV with four different combinations of drive systems among in-wheel motors and differential ones. To find out the best EV drive system configuration, it is adopted an optimisation process by means of a genetic algorithm that defines the electric motors (EMs) torque curves and powertrain transmission ratio in order to improve vehicle travel range and performance. The vehicle power demand is divided between the drive systems following rules established by the power management control which aims to reduce the lithium-ion battery discharges during the driving cycles: FTP-75 (urban driving), HWFET (highway driving) and US06 (high speeds and accelerations). After the simulations, the potential of each configuration is indicated according to its respective drive system and hence the best configurations are determined.

1 Introduction

The need for alternative energy sources to reduce CO_2 emission is one of the greatest challenges nowadays [1]. The unstable cost of petroleum, political dependence caused by imported resources and the stringent fuel-efficiency standards increase the demand for electric and hybrid vehicles [2]. Therefore, more attention has been given to researches on this kind of vehicles [3].

There are several configuration models of electric vehicles (EVs) and, in certain conditions; these ones are more suitable than others considering the advantages and disadvantages of each. In this paper, four different EVs configurations with two different ways of electric motors (EMs) coupling as proposed by [4, 5] are studied. They can be observed in Fig. 1.

In the first configuration (EV1), there are four EMs coupled directly to the vehicle wheels (in-wheel EMs) similar to described by Sakai *et al.* [6]. In the second configuration (EV2), two EMs are coupled to differential systems that increase the EMs speed and the final output torque at the vehicle wheels. This configuration is modelled according to Mutoh *et al.* [7, 8] that propose independent driving systems to be connected to the front and the rear wheels. The other configurations are combinations of the last two. Thus, the third configuration (EV3) represents the EMs coupled directly to the front wheels while the rear wheels having a differential system. Finally, the fourth configuration (EV4) has its vehicle front wheels propelled by an EM coupled to a differential system and its rear wheels being driven by two in-wheel EMs.

In the simulations, the EMs' power is provided by lithium-ion batteries that were chosen because of their high energy densities and long lifetime [9]. With respect to the EMs, they were used the brushless DC ones due to their low weight, high efficiency and compact size what make them as an interesting option for EV propulsion systems [10].

In previous work [11], it was studied the minimum battery size for an EV (with two independent drive systems) submitted to the standard Brazilian urban driving cycle NBR6601 [12]. Since the EVs normally have a limited autonomy range (100–200 km) [13], the study presented in [5] evaluates the travel range for the EV1,

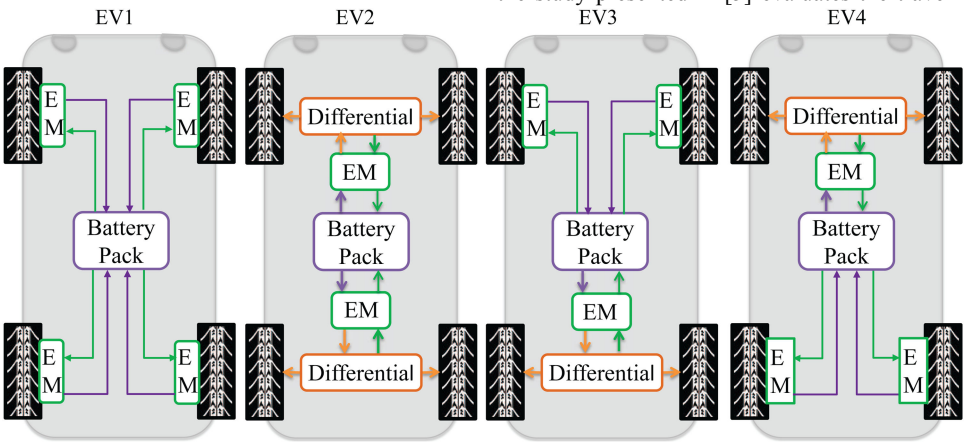

Fig. 1 *EV configurations*

© The Institution of Engineering and Technology 2016

EV2 and EV3 configurations (Fig. 1) according to the combination of three available EMs (5, 12 and 30 kW). In addition, this paper aims to optimise the EV travel distance by defining the optimum EM/drivetrain configuration that reduces the battery discharges without decreasing the vehicle performance during a combined driving cycle. This driving cycle represents a mix of different profiles: FTP-75 (urban driving), HWFET (highway driving) and US06 (high speeds and accelerations) [14]. Moreover, an estimated range of EV is obtained from Simulink/Matlab™ after simulating the battery discharge and travelled distance on previous driving cycle.

2 Vehicle longitudinal dynamics

To evaluate the longitudinal dynamic behaviour of the vehicle, it is implemented the equations proposed by Gillespie [15] for a conventional vehicle propelled by means of an engine/powertrain system with some available transmission ratio. Nevertheless, the equations are adapted for an EV configuration. The model is based on the movement resistance forces as the rolling and climbing resistance, aerodynamic drag and vehicle acceleration.

The rolling resistance (R_x) is related to the energy lost by the tire deformation and adhesion on contact area. At low speeds, the rolling resistance is the main resistance load, and it is estimated by (1) as a function of the vehicle weight (W) (N), multiplied by a dimensionless rolling resistance coefficient that expresses the effects of the interdependent physical properties of tire and ground [15] as a function of the vehicle speed (V) (m/s)

$$R_x = W\left(0.01 + 2.24 \times 10^{-4} V\right) \tag{1}$$

The air resistance against the car passage is named aerodynamic drag (D_A). This resistance force is defined by the air density (ρ) (kg/m^3), vehicle frontal area (A) (m^2) and an empirical constant based on the vehicle geometry known as drag coefficient (C_D) as shown in the following equation:

$$D_A = \frac{1}{2}\rho V^2 C_D A \tag{2}$$

The climbing resistance represents the road grade influence in the vehicle dynamics. Since the road grade is considered null in the simulated driving cycles, the climbing resistance is disregarded in the calculations.

As told before, the analyses considered four different EV combinations for propelling. The first (EV1) consists of in-wheel motors coupled directly to the vehicle wheels without any transmission system. The requested torque (T_{req}) for this configuration is shown in (3) as a function of the vehicle acceleration (a_x) (m/s^2), mass M (kg), the tire external radius (r) (m) and the wheels and tires inertia (I_W) (kgm^2) in which are also considered the in-wheel motors inertia

$$T_{req} = \left(Ma_x + \frac{I_w a_x}{r^2} + R_x + D_A\right) r \tag{3}$$

The second propulsion system configuration (EV2) consists of EMs coupled to differential transmission systems. In this case, the requested torque (T_{req}) is defined by (4) considering the differential inertia (I_d) (kgm^2) and transmission ratio (N_d) of the frontal ($_F$) and rear ($_R$) drive systems

$$T_{req} = \left(Ma_x + (I_{dF}N_{dF}^2 + I_{dR}N_{dR}^2 + I_w)\frac{a_x}{r^2} + R_x + D_A\right) r \tag{4}$$

The configurations EV3 and EV4 are a combination of EV1 and EV2, which one of the propulsion systems is composed of two in-wheel EMs, and the another one is a single EM coupled to a differential transmission. In both cases, the T_{req} is defined as

$$T_{req} = \left(Ma_x + (I_{d(F/R)}N_{d(F/R)}^2 + I_w)\frac{a_x}{r^2} + R_x + D_A\right) r \tag{5}$$

The total requested torque T_{req} (Nm) is evaluated by the power management control (PMC) according to the EV configuration (Fig. 1). Then, the PMC splits T_{req} between the rear [T_R (Nm)] and front [T_F (Nm)] propulsion systems, in order to keep the overall system running in the maximum available energy efficiency, without compromising the EV performance

$$T_{req} = T_F + T_R \tag{6}$$

If the propulsion system ($_R/_F$) is assembled in-wheel, the EM requested power is divided equally between both EMs as shown in (7). When the drive system is supported by a differential system, the requested torque is divided by the differential transmission ratio N_d and the mechanical efficiency (η_d) according to (8)

$$T_{IW(F/R)} = \frac{T_{(F/R)}}{2} \tag{7}$$

$$T_{Dif(F/R)} = \frac{T_{(F/R)}}{N_{d(F/R)}\eta_d} \tag{8}$$

According to Gillespie [15], the vehicle acceleration is limited by the available driving power and restricted by the tire traction. Thus, the PMC needs to consider the tire transmissible traction force in the definition of T_F and T_R to avoid performance losses. The vehicle traction limit is modelled as proposed by Jazar [16], that takes into consideration the weight transferred during the vehicle acceleration and the tire-ground peak coefficient of friction μ

$$T_{F(max)} = \mu\left(\frac{Mgc}{2L} - \frac{Mha_x}{2L}\right) r \tag{9}$$

$$T_{R(max)} = \mu\left(\frac{Mgb}{2L} + \frac{Mha_x}{2L}\right) r \tag{10}$$

where L is the vehicle wheelbase (m); h is the vehicle gravity centre height (m); g is the gravity acceleration (m/s^2); b is the longitudinal distance between the vehicle front axle and the gravity centre (m); and c is the longitudinal distance between the vehicle rear axle and the gravity centre (m).

3 Simulation parameters

The simulated EV presents dimensions similar to a conventional vehicle studied in [17]. The parameters applied in the simulations are shown in Table 1. As previously mentioned, when the EM is used in-wheel, its inertia is added to the wheels and tires inertia (I_w). When the EM is coupled to the differential system, an equivalent inertia (I_d) is considered. These inertias values change according to the EM power defined by the optimisation process and they are interpolated based on reference standard values.

4 Driving cycle

The driving profiles depend on a considerable parameter set such as traffic condition, topography and characteristics of the driver [2]. The driving cycle is established to represent the driver behaviour in the simulations. The requested vehicle acceleration (a_x) is defined by the difference between the current vehicle speed and the proposed velocity profile. In this paper, the EV performance and battery state of charge (SoC) are evaluated facing a combination of three cycles which represent different driving conditions. The FTP-75 urban cycle (Fig. 2*a*) denotes a low power demand and several short acceleration sections. The HWFET cycle (Fig. 2*b*) represents a long highway at high speed, and the US06 cycle (Fig. 2*c*) is characterised by high acceleration sections that increase the battery discharges. In high acceleration sections, the

© The Institution of Engineering and Technology 2016

20429746, 2017, 1, Downloaded from https://ietresearch.onlinelibrary.wiley.com/doi/10.1049/iet-est.2016.0022, Wiley Online Library on [08/02/2024]. See the Terms and Conditions (https://onlinelibrary.wiley.com/terms-and-conditions) on Wiley Online Library for rules of use; OA articles are governed by the applicable Creative Commons License

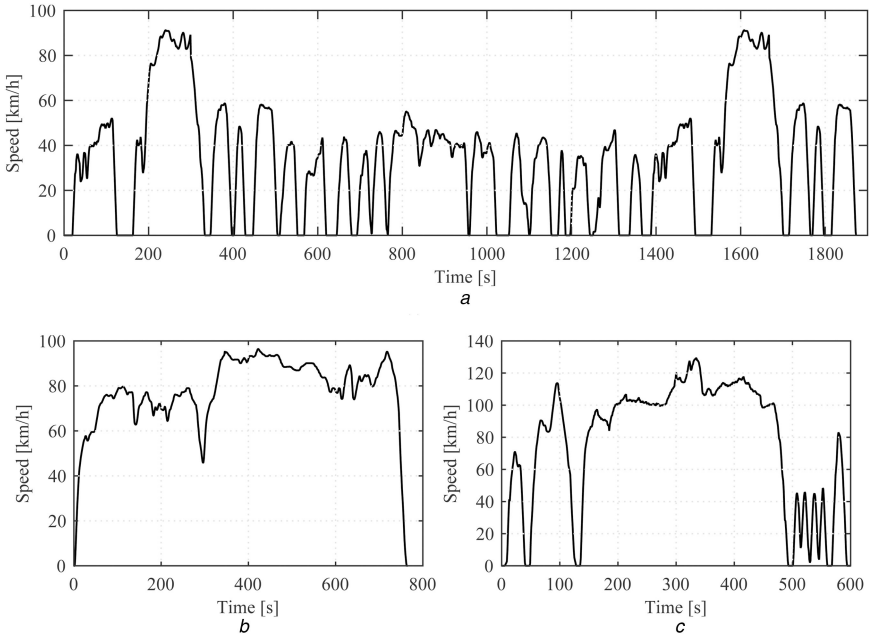

Fig. 2 *Standards driving cycles adapted from [14]*
(*a*) FTP-75, **(*b*)** HWFET, **(*c*)** US06

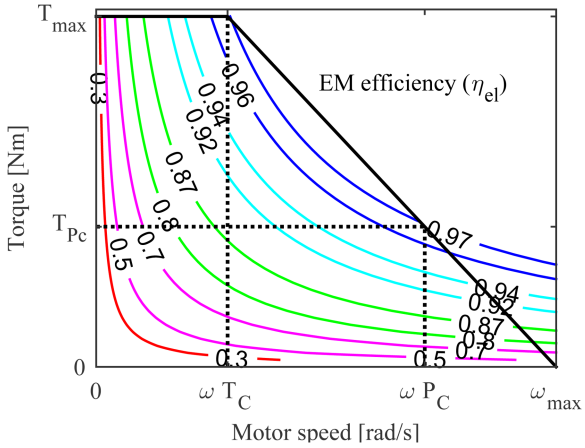

Fig. 3 *Electric motor efficiency map and torque curve*

tire traction limit strongly influences the vehicle acceleration performance and, consequently, the PMC power distribution between the rear and front drive systems.

5 Battery, electric motors and inverters

The Simulink™ database lithium-ion battery was used to simulate a 300 kg battery model with nominal voltage of 400 V according to Sanfélix *et al.* [18]. The battery life cycle can be dramatically reduced when the batteries discharge completely [19], and by this way the battery SoC must be limited [20]. The SoC is a measure of the capacity available compared with the full SoC [21]. In the simulations, the battery SoC is limited to 40% as adopted by Silva *et al.* [11] and Eckert *et al.* [20].

Table 1 Simulated vehicle parameters [17]

Components	
total vehicle mass (M)	980 kg
wheels + tires inertia (I_w)	2 kgm^2
differential efficiency (η_{fd})	0.9
vehicle frontal area (A)	1.8 m^2
drag coefficient (C_D)	0.33
tires 175/70 R13 radius (r)	0.2876 m
tire peak friction coefficient (μ)	0.9
wheelbase (L)	2.443 m
gravity centre height (h)	0.53 m
front axle to gravity centre (b)	0.983 m
rear axle to gravity centre (c)	1.460 m

In this work, it is not used a mathematical model for electric motors, but rather a motor torque curve. The EM current consumption I (A) is determined by (11), according to the requested torque ($T_{EM} = T_{IW}$ or $T_{EM} = T_{Dif}$), the EM speed ω_{EM}, the battery voltage V (V) and the inverter (η_{inv}) and EM (η_{el}) efficiencies

$$I = \frac{T_{EM}\omega_{EM}}{V\eta_{el}\eta_{inv}} \tag{11}$$

Equation (11) is applied to the front and the rear propulsion systems, once the EMs and inverter efficiency vary according to the EM torque curve and EM coupling configuration. The sum of the requested current I of both propulsion systems EMs is sent to the battery, reducing the battery SoC. Since the EMs torque curves are modified according to the optimisation process results, the EM torque curve and efficiency map used in the simulations is determined according to Fig. 3.

The optimisation algorithm determines the EM maximum torque T_{max} and the final speed of the constant torque phase (ω_{Tc}). According to Tong [22], the best operation point for the EM is located on the constant power phase running with torque between 10 and 30% of the maximum torque T_{max}. On the basis of these values, a second point of the torque curve is defined according to the recommended upper limit (30% T_{max}). Once the torque T_{Pc} is determined in (12), the EM speed ω_{Pc} can be calculated by the EM power (that is considered constant in this operation region) as shown in (13)

$$T_{Pc} = 0.3T_{max} \tag{12}$$

$$\omega_{Pc} = \frac{T_{max}\omega_{Tc}}{T_{Pc}} \tag{13}$$

The EM maximum speed (ω_{max}), where the EM torque becomes null, is defined as a linear progression of the two defined points. The EM efficiency η_{el} map is interpolated as a function of the

© The Institution of Engineering and Technology 2016

20429746, 2017, 1, Downloaded from https://ietresearch.onlinelibrary.wiley.com/doi/10.1049/iet-est.2016.0022, Wiley Online Library on [08/02/2024]. See the Terms and Conditions (https://onlinelibrary.wiley.com/terms-and-conditions) on Wiley Online Library for rules of use; OA articles are governed by the applicable Creative Commons License

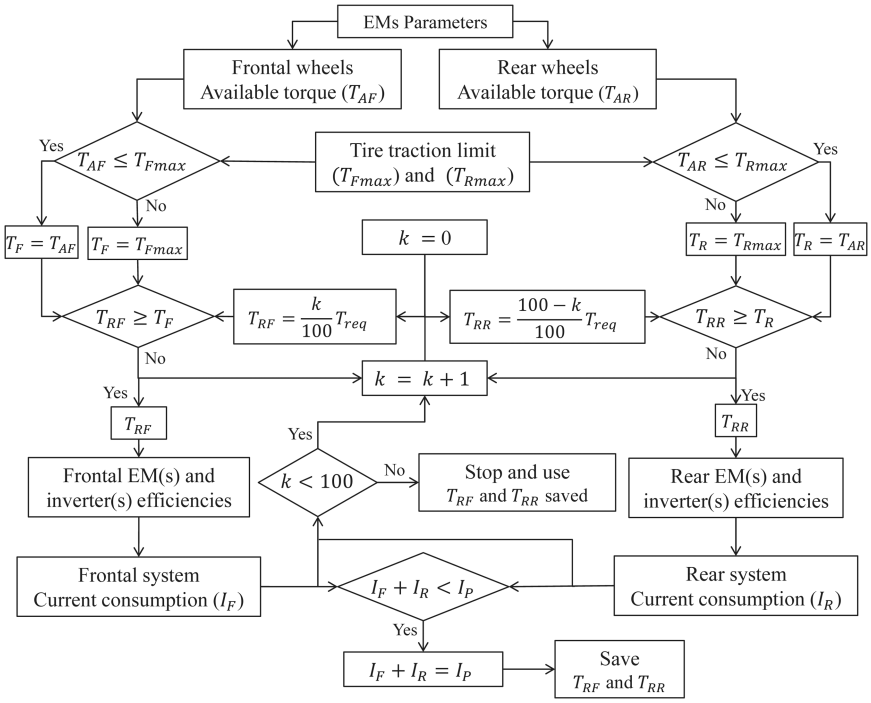

Fig. 4 *PMC algorithm*

defined EM torque curve. The inverter efficiency η_{inv} is also estimated based on Table 2.

5.1 Regenerative braking

The regenerative braking system allows the vehicle to recover the kinetic energy during deceleration [24]. When the vehicle is braking, the EMs are controlled to operate as a generator, converting the vehicle kinetic energy into electricity that is stored in the battery. This energy is then used in future accelerations [25].

The EM regeneration capacity is limited to 5% of a maximum torque curve of each EM according to Corrêa *et al.* [5]. When the EMs are regenerating at the maximum capacity, the residual brake torque (to keep the vehicle at the cycle requested speed) is provided by a friction of the mechanical brake system to guarantee the vehicle deceleration performance [26]. In this paper, the mechanical brake system is based only on the negative requested torque of (3), (4) or (5). According to Tara *et al.* [27], the battery charging can only be done below the maximum charging current.

6 Power management control

The EV PMC analyses the vehicle requested torque (T_{req}), estimated in function of the motion resistance forces provided by (3), (4) or (5) according to the EV configuration, and splits it between the front and rear drive systems according to the available torque at the wheels for each system (T_{AF} and T_{AR}). Each EM presents an efficiency map (Fig. 3) which is associated with the power inverter that also has a respective efficiency map (Table 2). These maps vary according to the EMs torque curves defined by the optimisation algorithm results.

To ensure that the EMs/inverters are operating in the best possible regime (that minimises the battery discharge) it is proposed a strategy that analyses all possible divisions of power between the front and rear axles. This power split is executed in a discrete way by a loop (1% of variation among the T_{req} split possibilities). Therefore, the current necessary to supply each power set is calculated, and the option that produces the smallest current is chosen. The control results in an output torque that keeps the vehicle at the desired speed with the minimum battery discharge and according to the propulsion system efficiency and also the EM coupling configuration.

The PMC also considers the maximum transmissible torque (T_{Fmax} and T_{Rmax}) related to tire-road conditions to avoid performance losses by sending more torque than the contact between tire and ground can transmit. In other words, the PMC shares the power between the available drive systems in proportion to the minimum consumption of current [I (A)] and among all possibilities that does not overcome the respective propulsion system tires traction limit.

Fig. 4 shows the PMC control to minimise the battery discharges. It can be seen that other possibilities are considered in the PMC algorithm, for example, the use of the maximum possible torque from one of the drive systems T_{F} or T_{R} (after evaluating the tire traction limits) and also the complementation of the remaining torque by the other propulsion system when it is necessary ($T_{\text{R(F/R)}} = T_{\text{req}} - T_{\text{(R/F)}}$). If the sum of the available torques from both propulsion systems becomes lower than the requested torque ($T_{\text{F}} + T_{\text{R}} < T_{\text{req}}$), the PMC uses the maximum available torques, disregarding the energy efficiency, and so trying to reach a better performance along the driving cycle.

Table 2 Inverter efficiency map adapted from [23]

	ω_{EM}, rad/s				
T_{EM}, Nm	$0.1\omega_{\text{Pc}}$	$0.3\omega_{\text{Pc}}$	$0.5\omega_{\text{Pc}}$	$0.7\omega_{\text{Pc}}$	ω_{Pc}
0	0.65	0.84	0.90	0.84	0.83
$0.11T_{\text{max}}$	0.74	0.89	0.94	0.91	0.91
$0.33T_{\text{max}}$	0.82	0.93	0.96	0.96	0.96
$0.56T_{\text{max}}$	0.83	0.94	0.97	0.97	0.97
T_{max}	0.83	0.94	0.97	0.97	0.97

© The Institution of Engineering and Technology 2016

20429746, 2017, 1, Downloaded from https://ietresearch.onlinelibrary.wiley.com/doi/10.1049/iet-est.2016.0022, Wiley Online Library on [08/02/2024]. See the Terms and Conditions (https://onlinelibrary.wiley.com/terms-and-conditions) on Wiley Online Library for rules of use; OA articles are governed by the applicable Creative Commons License

7 Optimisation problem formulation

The purpose of the optimisation is to minimise the battery discharges by establishing the most efficient EV configuration. It is important to highlight that lower power EMs minimise the battery discharges, however they decrease the vehicle performance because they cannot meet the requested power to follow the driving cycle speed.

The vehicle performance is evaluated by means of the correlation coefficient R [17, 20]. It compares the simulated vehicle speed with the standard driving cycles according to (14) where V_{ci} represents the cycle speed at discrete time points, V_i refers to the simulated vehicle speed, and $\bar{V}$ and $\bar{V}_c$ are associated mean values. The perfect match between the simulated speed profile and the standard cycle results in $R = 1$, what means that the vehicle may follow the requested speed profile in all cycle sections

$$R^2 = \frac{\left(\sum (V_{ci} - \bar{V}_c)(V_i - \bar{V})\right)^2}{\sum (V_{ci} - \bar{V}_c)^2 \sum (V_i - \bar{V})^2} \tag{14}$$

The objective functions for a bi-criteria optimisation process are defined to maximise the final battery SoC (f_1) and also to maximise the vehicle performance R (f_2)

$$\max\ f_1(X) = \mathrm{SoC}(X) \tag{15}$$

$$\max\ f_2(X) = R(X) \tag{16}$$

Subject to: constrains C presented in (17). These constrains represent the battery discharge limit, EMs and powertrain restrictions

$$C(X) = \begin{cases} \mathrm{SoC} \geq 40\% \\ 10 \leq T_{\max} \leq 200 \\ 250 \leq \omega_{\mathrm{Tc}} \leq 5000 \\ 3.5 \leq N_{\mathrm{d}} \leq 7 \end{cases} \tag{17}$$

As previously mentioned, smaller EMs present lower power consumption, however, the minimisation of the EMs by the optimisation process, may generate EV configurations with a long drive range, but with a poor performance especially in the high speed sections. To avoid this, the vehicle performance is also used as a constrain and, the EV performance should be at least equal to the performance ($R \geq 0.9842$) reached from the conventional 1.0 l combustion engine vehicle simulated in [17], which is submitted to the same driving cycles studied in this paper. Simulation results with lower performance like the conventional vehicle are disregarded in the optimisation process.

8 Interactive adaptive-weight genetic algorithm (i-AWGA)

To solve the optimisation problem, the i-AWGA is implemented as proposed by Gen *et al.* [28] with an improvement of the AWGA [29] and considering a penalty fitness (Ft) value for the dominated solutions.

8.1 Design variables

The input parameters for the rear and front drive systems are gathered in a chromosome X as shown in (18). where the variable N_{EMs} represents the quantity of electric motors used ($N_{\mathrm{EMs}} = 2$ refers to in-wheel motors and $N_{\mathrm{EMs}} = 1$ refers to single EM combined with the differential system)

$$[X] = [T_{\max\mathrm{F}} \quad \omega_{\mathrm{TcF}} \quad N_{\mathrm{EMsF}} \quad N_{\mathrm{dF}} \quad T_{\max\mathrm{R}} \quad \omega_{\mathrm{TcR}} \quad N_{\mathrm{EMsR}} \quad N_{\mathrm{dR}}] \tag{18}$$

For the in-wheel configuration, the transmission ratio N_{d} is considered equal to 1 in the same way that the mechanical efficiency of the transmission η_d is equal to 1 because the EMs are connected directly to the vehicle wheels. On the other hand, when the EM is coupled to the differential system, the transmission ratio is defined according to the constrains C (17) and the efficiency of η_d becomes equal to 0.9.

8.2 Ft adaptive weight approach

The Ft value is defined by weighted-sum approach, to avoid inaccuracy in the definition of appropriate weights that are difficult to determine [29]. The adaptive weight approach defines weight values according to the maximum ($z_k^{\max}$) and minimum ($z_k^{\min}$) values of each optimisation criteria (k) for the Ft value $f_k(X)$ ($1 \leq k \leq 2$) of one solution X in the population (P)

$$z_k^{\max} = \max\ \{f_k(X) | (X) \in P\} \tag{19}$$

$$z_k^{\min} = \min\ \{f_k(X) | (X) \in P\} \tag{20}$$

The adaptive weight method readjusts the weight ($w_i(X)$) values for each population member ($1 \leq i \leq N$), as shown in (21) for a maximisation problem

$$w_i(X) = \sum_{k=1}^{2} = \frac{f_{k(i)}(X) - z_k^{\min}}{z_k^{\max} - z_k^{\min}} \tag{21}$$

A penalty value $p_i(X)$ is added in the Ft value, according to the frontier of non-dominated compromised solutions (Pareto-rank of $P_{\mathrm{r}}(X) = 1$) between the optimisation criteria f_1 and f_2. For the maximisation problem, the penalty values are defined as

$$p_i(X) = \begin{cases} 1 & \text{if } P_{\mathrm{r}(i)}(X) = 1 \\ 0 & \text{if } P_{\mathrm{r}(i)}(X) > 1 \end{cases} \tag{22}$$

The final Ft value is defined by the sum of the adaptive weigh $w(X)$ with the penalty value $p(X)$ as shown in (23), and the population is ordered in function of the fitness Ft(i) values

$$\mathrm{Ft}(i) = w_i(X) + p_i(X) \tag{23}$$

8.3 Selection

The roulette wheel technique is applied to the selection of the population members for the genetic algorithm (GA). For each population member (i), it is assigned a roulette-wheel slot proportional to its Ft value Ft(i). The selection probability $S_{\mathrm{P}}(i)$ is defined in (24) by the sum of Ft values for all the population members ($1 \leq j \leq N$)

$$S_{\mathrm{P}}(i) = \frac{\mathrm{Ft}(i)}{\sum_{j=1}^{N} \mathrm{Ft}(j)} \tag{24}$$

This probability defines a numerical interval used in the selection process as shown in the following equation:

$$q(i) = \sum_{j=1}^{i} S_{\mathrm{P}}(j) \tag{25}$$

The selection algorithm chooses two different population members (M_1 and M_2) defining a random value $r \in (0, 1]$. If $r < q_i$ the first population member chromosome is selected, otherwise the population members selection is defined as $q_{i-1} < r < q_i$.

8.4 Crossover and mutation process

The crossover operator combines the selected members M_1 and M_2 and the chromosomes [X] to generate two new set of parameters to perform a new simulation. The first combined chromosome keeps the frontal propulsion system from M_1 and the rear driving system

© The Institution of Engineering and Technology 2016

20429746, 2017, 1, Downloaded from https://ietresearch.onlinelibrary.wiley.com/doi/10.1049/iet-est.2016.0022, Wiley Online Library on [08/02/2024]. See the Terms and Conditions (https://onlinelibrary.wiley.com/terms-and-conditions) on Wiley Online Library for rules of use; OA articles are governed by the applicable Creative Commons License

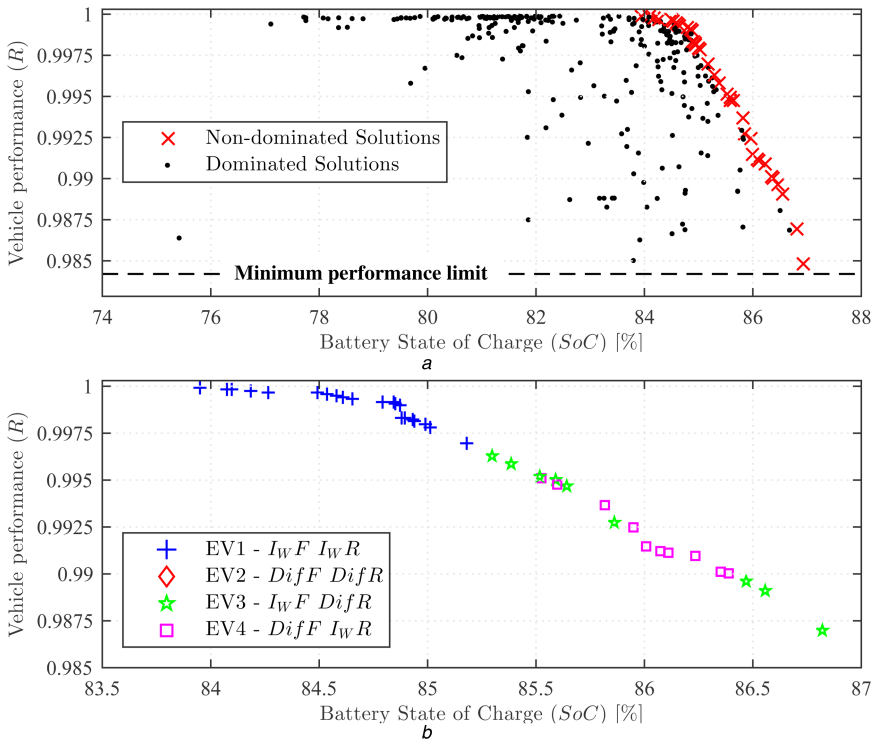

Fig. 5 *GA simulation results*
(a) Pareto frontier, ***(b)*** EV configurations of the non-dominated solutions

from M_2. The second combined chromosome uses the frontal system from chromosome M_2 and the rear system from M_1. The new simulations are then performed and the results are stored in the population database.

To insert different parameters values into the population, the mutation operator changes some of the design variables of the chromosomes generated by the crossover process. The mutation operator defines randomly the variables that will mutate by setting a random value ($v_p \in [0, 1]$) for each design variable using the Matlab function *rand*. In case of $v_p < 0.5$, the design variable maintains the original value and if $v_p \geq 0.5$, the variable value is mutated by adding a random value MT according to the mutation limits (Table 3) defined for each design variable. If one of the mutated parameters does not respect the defined constrains, as presented in (17), or the generated chromosome does not present mutation in any of the variables, this chromosome is discarded and a new mutation process is performed until finding a mutated chromosome that agrees with the constrains C.

The last mutation possibility is to change the EV configuration by inverting the rear and front propulsion systems. This will change the vehicle behaviour because of the tire traction limits that are different for the frontal and rear wheels. Then, the mutation process generates two new chromosomes, which are simulated and the results are added to the population. The new EMs and differential inertias are rearranged according to the new mutated values that were defined.

Table 3 Mutation limits for each propelling system

Crossover variable values	Mutation $v_p \in [0, 1]$		Mutated variables
	if $v_p < 0.5$	if $v_p \geq 0.5$	
T_{max}	MT = 0	−50 < MT < 50	T_{max} + MT
ω_{Tc}	MT = 0	−500 < MT < 500	ω_{Tc} + MT
N_d (only to differential configurations)	MT = 0	−1 < MT < 1	N_d + MT

8.5 Population and convergence criteria

The initial population is composed of 40 members with randomly generated chromosomes [X]. The population enlarges by the addition of the crossover and mutation results. To control the population size, the last Pareto rank results are eliminated when the population size reaches $P_{Lim} = 50$ members. If the non-dominated population ($\Pr(X) = 1$) reaches the P_{Lim}, the population limit is redefined as $P_{Lim} = P_{Lim} + 50$. The algorithm stops when the Pareto frontier remains the same for over ten crossover/mutations sets of simulations.

9 Results

The convergence of the GA algorithm ends in a set of non-dominated solutions that are defined as Pareto frontier. Fig. 5*a* shows all the results, generated by the GA algorithm, that present performance above the minimum performance limit ($R = 0.9842$). The EV configurations that compose the Pareto frontier of non-dominated solution are shown in Fig. 5*b* in which it can be observed that only the EV configurations EV1, EV3 and EV4 are in the frontier, furthermore these configurations also demonstrate performance and final SoC better than EV2 configuration.

To perform a comparative analysis, three results from the Pareto frontier were selected: the maximum performance (R) reached by an EV1 configuration, the maximum SoC of the battery that was performed by an EV3 configuration and also the solution with the higher Ft value reached by an EV1 configuration and showing the best compromised solution. Table 4 shows the results reached by these configurations.

Table 4 Selected solutions results

EV configuration	Solutions	Performance R	Final battery SoC, %	Fitness Ft	Travelled distance, km	Estimated drive range, km
EV1	maximum R	0.9999	83.95	2.84	47.17	176.30
EV3	maximum SoC	0.9848	86.93	2.66	44.28	203.35
EV1	maximum Ft	0.9991	84.84	2.87	46.97	185.90

© The Institution of Engineering and Technology 2016

20429746, 2017, 1, Downloaded from https://ietresearch.onlinelibrary.wiley.com/doi/10.1049/iet-est.2016.0022, Wiley Online Library on [08/02/2024]. See the Terms and Conditions (https://onlinelibrary.wiley.com/terms-and-conditions) on Wiley Online Library for rules of use; OA articles are governed by the applicable Creative Commons License

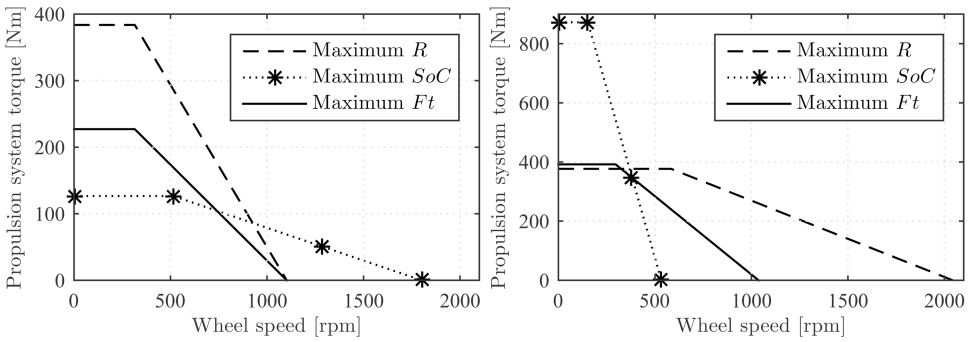

Fig. 6 *Optimised EMs torque curves according to the EV configuration*
(*a*) Front EMs, **(*b*)** Rear EMs

The maximum performance result ($R = 0.9999$) followed the cycles requested speed in all sections and its travelled distance was the same as the sum of the three cycles that is 47.17 km. In the other hand, the maximum SoC solution presented a lower battery discharge and it was not able to fulfil the cycle speed profile in some stretches, showing a performance decrease and, consequently, a lower travelled distance.

The configuration EV4 is also an alternative for a compromised solution between vehicle performance and battery SoC. This configuration presented solutions mixed with the EV3 configuration in the Pareto frontier (Fig. 5*b*) because both of them used in-wheel EMs at least in one drive system and a single EM coupled to a differential reduction in the other propel system. With the correct combination among the design variables and PMC for these configurations it was possible to find out possible optimum solutions.

The EV drive range was estimated from the vehicle travelled distance and also by the battery SoC to perform the driving cycles. The drive range consists in the repeatability of these speed profiles until the battery reaches the minimum allowed SoC (SoC = 40%). A configuration that prioritises performance presents a travel distance close to the requested by the cycle, but also presents higher battery discharges that results in a lower drive range compared with EV configurations that aim to save the battery power, even if the EV remains unable to keep the requested speed in some section reducing the travelled distance as compared with the standard cycles.

The EMs parameters from the selected solutions are shown in Table 5.

There are different ways to couple the EM to vehicle wheels, Fig. 6 shows the available torque at the vehicle wheels. The in-wheel EMs torque is multiplied by two, because there is one EM in each wheel thus two wheels/motors for each independent propulsion system. Among the selected results only the maximum SoC presents a differential transmission associated with an EM, to propel the EV rear system (EV3) and, in this case, the EM output torque is multiplied by the differential transmission ratio ($N_d = 6.42$) and also by a mechanical efficiency factor ($\eta_d = 0.9$).

The EV battery behaviour during the simulated driving cycles is shown in Fig. 7*a*. It is possible to observe that the battery SoC presents a lower curve decrease in the FTP-75 cycle. It happens because the urban driving presents a lower speed with a moderate requested power and also many small sections where the EV is not moving (no battery discharges). The next cycle, (HWFET) highway behaviour, presents a higher battery discharge because the requested power increases due to the aerodynamic drag that represents the major parcel of the vehicle movement resistance forces in highway drive condition (high speed and low acceleration). When the EV reaches the US06 cycle, the battery presents the largest discharges due to the high speeds as in the HWFET cycle and also because of the high acceleration section that requires a large amount of power from the battery to keep the vehicle at the requested speed and also, in this section, the most of configurations using both propulsion systems become closer to the maximum output torque.

Fig. 7*b* shows the battery SoC discharge rate (%/s). There are only few small positive points that indicate regenerative braking. These points are associated with the long braking sections of the cycles, however, it cannot provide expressive changes in the battery SoC. It happens basically because of the high battery capacity that is necessary to provide power to the EMs that request an amount of power several times more than its regenerative capacity.

Moreover, in Fig. 7*b* it is possible to observe that the maximum Ft and maximum SoC solution present lower discharge rates as compared with the maximum *R* solution in the US06 cycle. The maximum SoC presents less discharge in the HWFET cycle section. These differences occur because of the drive torque limits, in other words, configurations that aim to save battery charge use smaller EMs that operate its better efficiency in the urban behaviour and it represents the largest part of the EV operation time in the simulated cycles.

However, when the EV reaches the high speed sections these optimised EMs for urban cycle are operating at a constant power phase where the output torque decrease with the EM speed increase. Therefore, when the request torque T_{req} becomes superior to the sum of the available torques for both propulsion systems (at high speed the tire traction is not the vehicle acceleration limiter), the vehicle is unable to increase the velocity and the EV performance decrease, thus it remains at a constant speed limit until the requested power decreases. Fig. 8 shows the difference among the solutions in the sections where the EVs present performance losses.

The maximum performance solution represents the cycle request speed. Also, it is possible to observe that the maximum Ft solution is limited to 115 km/h and the minimum SoC configuration is limited to 88 km/h at maximum speed. All the results of this paper present better performance as compared with a single power source low power conventional vehicle propelled by an engine associated to a 5 ratio gearbox and differential system simulated in [17]. This is because the conventional vehicle presents a performance decrease by the clutch decoupling during the several gear shiftings for the driving cycles and also due to the engine available power and tire transmissible torque at the high acceleration section of the US06 cycle.

Table 5 Selected solutions chromosomes

Propelling system	Front				Rear			
Chromosome *X*	T_{max}	ω_{Tc}	N_{EMs}	N_d	T_{max}	ω_{Tc}	N_{EMs}	N_d
maximum *R*	191.86	314.9	2	1	188.45	583.7	2	1
maximum SoC	63.28	514.8	2	1	150.96	978.6	1	6.42
maximum Ft	113.55	314.9	2	1	196.03	296.3	2	1

© The Institution of Engineering and Technology 2016

20429746, 2017, 1, Downloaded from https://ietresearch.onlinelibrary.wiley.com/doi/10.1049/iet-est.2016.0022, Wiley Online Library on [08/02/2024]. See the Terms and Conditions (https://onlinelibrary.wiley.com/terms-and-conditions) on Wiley Online Library for rules of use; OA articles are governed by the applicable Creative Commons License

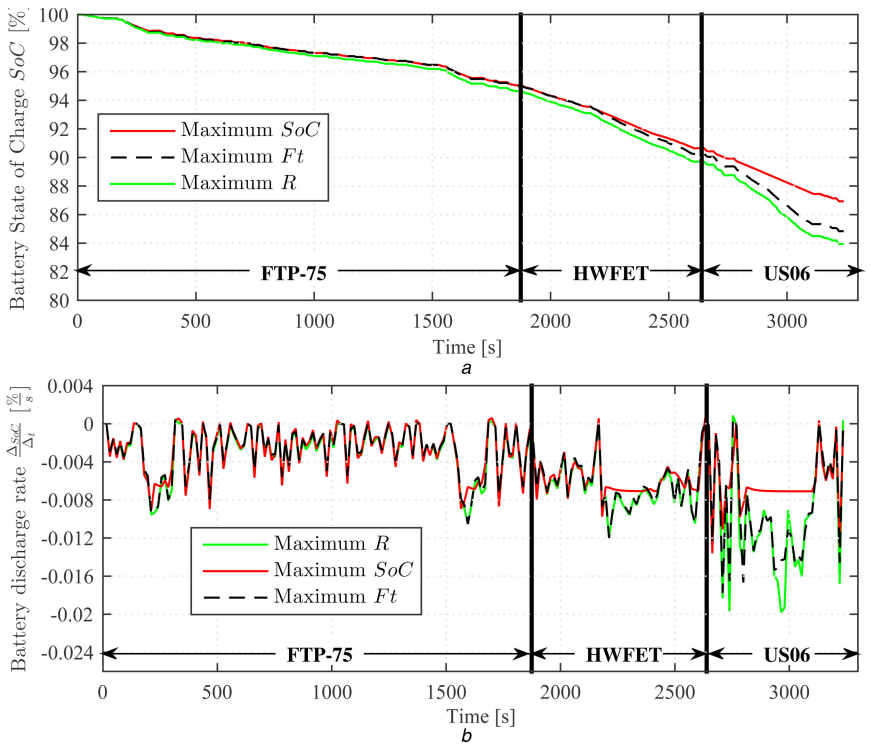

Fig. 7 *Battery SoC comparative among the analysed EV configurations in the simulated cycles*
(*a*) Battery SoC during the driving cycles, **(*b*)** Battery discharge rate during the driving cycles

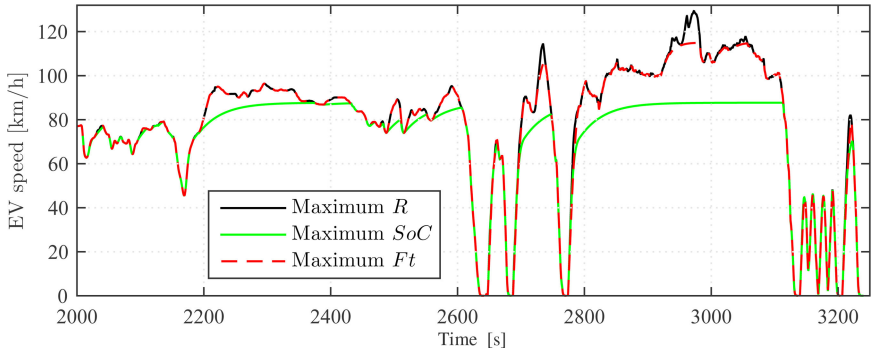

Fig. 8 *Performance comparative among the analysed EV configurations*

The EVs studied in this paper present performance limited by the EMs torque curve as mentioned previously, however other limitations are outlined. For example, the EVs are composed of two propulsion systems, therefore the tire traction limitation is mostly solved by transferring the power demand from the drive system, that exceeds the tire traction to the other one.

10 Conclusion

In this paper, it was studied the influence of the propulsion systems configurations in an EV. Four EV configurations were proposed and a GA was implemented to optimise the electric motors torque curves and define the configuration that presents the lower battery discharge (max SoC) without decreasing the vehicle performance under an acceptable limit.

The optimisation result, in a set of optimised compromised solutions, was composed of the configurations EV1 with four in-wheel EMs, and by EV3/EV4 configurations that associate two in-wheel EMs in one propulsion system and EM + differential in the other drive system. This configurations present better performance and battery SoC than the EV2 configuration that uses EMs + differential in both propel systems.

The solutions that present the best result for each optimisation criteria and the best compromised solution were selected. The battery and vehicle longitudinal behaviour were compared. The maximum performance solution was reached by an EV1 configuration that was able to fulfil the cycles requested speed in all the section, and it presented 176.3 km as an estimated drive range. The maximum SoC solution was achieved by an EV3 configuration that presented 203.35 km drive range representing 15.34% of improvement, however, this configuration showed a performance decrease that reduce the final travelled range in 6.13%, because these EV had a speed limit of 88 km/h making it unable to reach the cycle desired speed in some sections. Finally, the best compromised solution (maximum Ft) is also an EV1 that provides 185.9 km of drive range (5.45% more than the maximum performance and 8.58% less than the maximum SoC) with 0.42% decrease in the travelled distance as compared with the standard cycles and 115 km/h as maximum speed.

Finally, all the results and discussions have led to the design procedure that ensures all operating conditions for longitudinal dynamics. In future studies, optimised PMC will be implemented for each optimum drivetrain configuration. Also, advanced models will be developed including the lateral dynamics, therefore an overview about stability applied in EV configuration possibly will be held.

11 Acknowledgments

This work was conducted during scholarships supported by the Brazilian Federal Agency for Support and Evaluation of Graduate Education (CAPES), the National Council for Scientific and Technological Development (CNPq) and the State University of Campinas (UNICAMP)

© The Institution of Engineering and Technology 2016

20429746, 2017, 1, Downloaded from https://ietresearch.onlinelibrary.wiley.com/doi/10.1049/iet-est.2016.0022, Wiley Online Library on [08/02/2024]. See the Terms and Conditions (https://onlinelibrary.wiley.com/terms-and-conditions) on Wiley Online Library for rules of use; OA articles are governed by the applicable Creative Commons License

12 References

[1] Rahman, K.M., Patel, N.R., Ward, T.G., *et al.*: 'Application of direct-drive wheel motor for fuel cell electric and hybrid electric vehicle propulsion system', *IEEE Trans. Ind. Appl.*, 2006, **42**, (5), pp. 1185–1192

[2] Schwarzer, V., Ghorbani, R.: 'Drive cycle generation for design optimization of electric vehicles', *IEEE Trans. Veh. Technol.*, 2013, **62**, (1), pp. 89–97

[3] Liu, P., Liu, H.P.: 'Permanent-magnet synchronous motor drive system for electric vehicles using bidirectional z-source inverter', *IET Electr. Syst. Transp.*, 2012, **2**, (4), pp. 178–185

[4] Yuan, X., Wang, J.: 'Torque distribution strategy for a front-and rear-wheel-driven electric vehicle', *IEEE Trans. Veh. Technol.*, 2012, **61**, (8), pp. 3365–3374

[5] Corrêa, F.C., Eckert, J.J., Silva, L.C., *et al.*: 'Study of different electric vehicle propulsion system configurations'. Vehicle Power and Propulsion Conf. (VPPC), 2015, 2015

[6] Sakai, S.-i., Sado, H., Hori, Y.: 'Motion control in an electric vehicle with four independently driven in-wheel motors', *IEEE/ASME Trans. Mechatronics*, 1999, **4**, (1), pp. 9–16

[7] Mutoh, N., Kazama, T., Takita, K.: 'Driving characteristics of an electric vehicle system with independently driven front and rear wheels', *IEEE Trans. Ind. Electron.*, 2006, **53**, (3), pp. 803–813

[8] Kang, J., Yoo, J., Yi, K.: 'Driving control algorithm for maneuverability, lateral stability, and rollover prevention of 4WD electric vehicles with independently driven front and rear wheels', *IEEE Trans. Veh. Technol.*, 2011, **60**, (7), pp. 2987–3001

[9] Gao, L., Liu, S., Dougal, R.A.: 'Dynamic lithium-ion battery model for system simulation', *IEEE Trans. Compon. Packag. Technol.*, 2002, **25**, (3), pp. 495–505

[10] Yang, Y.-P., Chuang, D.S.: 'Optimal design and control of a wheel motor for electric passenger cars', *IEEE Trans. Magn.*, 2007, **43**, (1), pp. 51–61

[11] Silva, L.C., Eckert, J.J., Santiciolli, F.M., *et al.*: 'A study of battery power for a different electric vehicle propulsion system'. Int. Conf. on Electrical Systems for Aircraft, Railway, Ship Propulsion and Road Vehicles (ESARS), 2015, 2015

[12] NBR6601: 'Light road motor vehicles – Determination of hydrocarbons, carbon monoxide, nitrogen oxides, carbon dioxides and particulate matter in the exhaust gas', ABNT Std., October 2005

[13] Hofman, T., Dai, C.: 'Energy efficiency analysis and comparison of transmission technologies for an electric vehicle'. Vehicle Power and Propulsion Conf. (VPPC), 2010 IEEE, 2010, pp. 1–6

[14] Barlow, T.J., Latham, S., McCrae, I.S., *et al.*: *'A reference book of driving cycles for use in the measurement of road vehicle emissions'. TRL Published Project Report*, 2009

[15] Gillespie, T.D.: '*Fundamentals of vehicle dynamics*' (Society of Automotive Engineers – SAE, Warrendale, PA, USA, 1992)

[16] Jazar, R.N.: '*Vehicle dynamics. Theory and applications*' (Springer Science+ Business Media, New York, NY, USA: Springer, 2008)

[17] Eckert, J.J., Corrêa, F.C., Santiciolli, F.M., *et al.*: 'Vehicle gear shifting strategy optimization with respect to performance and fuel consumption', *Mech. Based Des. Struct. Mach.*, 2016, **44**, pp. 123–136

[18] Sanfélix, J., Messagie, M., Omar, N., *et al.*: 'Environmental performance of advanced hybrid energy storage systems for electric vehicle applications', *Appl. Energy*, 2015, **137**, pp. 925–930

[19] Fuhs, A.: '*Hybrid vehicles: and the future of personal transportation*' (CRC Press, 2008)

[20] Eckert, J.J., Santiciolli, F.M., Silva, L.C.A., *et al.*: 'Co-simulation to evaluate acceleration performance and fuel consumption of hybrid vehicles', *J. Braz. Soc. Mech. Sci. Eng. (BMSE)*, 2016, pp. 1–14, DOI: 10.1007/s40430-015-0484-4

[21] Tannahill, V.R., Sutanto, D., Muttaqi, K., *et al.*: 'Future vision for reduction of range anxiety by using an improved state of charge estimation algorithm for electric vehicle batteries implemented with low-cost microcontrollers', *IET Electr. Syst. Transp.*, 2014, **5**, (1), pp. 24–32

[22] Tong, W.: '*Mechanical design of electric motors*' (CRC Press, Broken Sound Parkway NW, Suite 300 Boca Raton, FL, 2014)

[23] Rotering, N., Ilic, M.: 'Optimal charge control of plug-in hybrid electric vehicles in deregulated electricity markets', *IEEE Trans. Power Syst.*, 2011, **26**, (3), pp. 1021–1029

[24] Lv, C., Zhang, J., Li, Y., *et al.*: 'Mechanism analysis and evaluation methodology of regenerative braking contribution to energy efficiency improvement of electrified vehicles', *Energy Convers. Manage.*, 2015, **92**, pp. 469–482

[25] Junzhi, Z., Yutong, L., Chen, L., *et al.*: 'New regenerative braking control strategy for rear-driven electrified minivans', *Energy Convers. Manage.*, 2014, **82**, pp. 135–145

[26] Zhang, J., Lv, C., Gou, J., *et al.*: 'Cooperative control of regenerative braking and hydraulic braking of an electrified passenger car'. Proc. Institution of Mechanical Engineers, Part D: Journal of Automobile Engineering, 2012, pp. 1289–1302

[27] Tara, E., Shahidinejad, S., Filizadeh, S., *et al.*: 'Battery storage sizing in a retrofitted plug-in hybrid electric vehicle', *IEEE Trans. Veh. Technol.*, 2010, **59**, (6), pp. 2786–2794

[28] Gen, M., Cheng, R., Lin, L.: '*Network models and optimization: multiobjective genetic algorithm approach*' (Springer Science & Business Media, Verlag London, 2008)

[29] Gen, M., Cheng, R.: '*Genetic algorithms and engineering optimization*' (John Wiley & Sons, Third Avenue 605, New York, NY, 2000), vol. **7**

© The Institution of Engineering and Technology 2016

20429746, 2017, 1, Downloaded from https://ietresearch.onlinelibrary.wiley.com/doi/10.1049/iet-est.2016.0022, Wiley Online Library on [08/02/2024]. See the Terms and Conditions (https://onlinelibrary.wiley.com/terms-and-conditions) on Wiley Online Library for rules of use; OA articles are governed by the applicable Creative Commons License